Applied Surface Science 689 (2025) 162564

Contents lists available at ScienceDirect

Applied Surface Science

journal homepage: www.elsevier.com/locate/apsusc

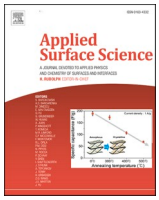

Full Length Article

Tuning the band gap in InSb (100) by surface chemical doping

Jingwei Dong [a,b], Yi Lian [c], Yongguang Zhang [a,b], Luca Perfetti [d,*], Zhongwei Chen [a,b,*]

[a] Power Battery & Systems Research Center, Dalian Institute of Chemical Physics, Chinese Academy of Sciences, Dalian 116023, PR China
[b] State Key Laboratory of Catalysis, Dalian Institute of Chemical Physics, Chinese Academy of Sciences, Dalian 116023, PR China
[c] Institute of Atomic and Molecular Physics, Jilin University, Changchun 130012, PR China
[d] Laboratoire des Solides Irradiés, CEA/DRF/IRAMIS, CNRS, Ecole Polytechnique, Institut Polytechnique de Paris, 91128 Palaiseau, France

ARTICLE INFO

Keywords:
Surface chemical doping
Interface dipole field
Optical material
Electronic Band Structure

ABSTRACT

Surface chemical doping is known to induce an interface dipole electric field, which has recently attracted considerable attention for its capacity to modulate the electronic and optical properties of semiconducting materials. InSb is considered one of the most promising semiconducting crystals due to its exceptional electron and hole mobility, surpassing that of other common III-V semiconductors. Here, we demonstrated the tuning of band gap renormalization in InSb (100) through *in situ* surface potassium atom doping, directly observed using time- and angle-resolved photoelectron spectroscopy. In addition, density functional theory calculations were performed to analyze the band gap evolution in InSb under the electric field perpendicular to the (100) crystal plane. Our study not only provides a clear observation of the band gap renormalization of InSb but also highlights its potential to enhance practical applications in contemporary photoelectric devices based on InSb.

1. Introduction

InSb is considered as an alternative semiconductor for silicon electron devices due to its exceptional electron mobility of roughly 7.7×10^4 $cm^2\ V^{-1}\ s^{-1}$ and narrow bandgap 0.18 eV at 300 K among III–V semiconductors [1–4]. InSb semiconductor's properties make it highly suitable for applications ranging from infrared detectors and thermoelectric devices to high-speed electronics and potentially quantum computing, contributing significantly to various technological advancements across different industries [5–10].

A narrower band gap means that the semiconductor requires less energy to move electrons from the valence band to the conduction band. This property greatly affects the material's electrical conductivity and enables low-energy consumption in integrated circuits. To enhance the optoelectronic properties of semiconductors, external fields are often used to manipulate and study their band gap renormalization. In-situ evaporation of alkali metal atoms onto the crystal surface will produce a surface dipole field, which is one of the most effective methods for studying the regulation of semiconductor electronic structure [11–13]. According to the data of Kang et al, a significant band gap renormalization of ~400 meV and indirect-to-direct band gap transitions is observed in layered transition metal dichalcogenides (TMDs) MX_2 (M = Mo, W; X = S, Se, Te) semiconductors by surface doping of Rb atoms [11]. Additionally, black phosphorus shows a semiconductor-to-metal phase transition through the closing of its band gap using surface alkali metal dopants [12,13].

In this study, we experimentally tracked the bandgap renormalization of InSb (100) by employing in situ surface electron doping along with time- and angle-resolved photoemission spectroscopy (TrARPES). TrARPES enables us to detect changes in the position of the valence band maximum (VBM) and conduction band minimum (CBM), allowing us to extract the band gap during early doping time [13–16]. At low doping densities, we observed only a common downward shift of the VBM and CBM, rather than a bandgap renormalization in energy space. With increasing doping time, a significant reduction in the band gap occurred at high doping densities. Moreover, density functional theory (DFT) calculations certify that the band gap shrink in InSb (100) can be achieved by applying the electric field perpendicular to the (100) crystal plane. We believe that our study will enable InSb semiconductors to have wide-ranging applications and provide valuable insights to enhance the optoelectronic properties of other semiconductor materials.

* Corresponding authors at: Power Battery & Systems Research Center, Dalian Institute of Chemical Physics, Chinese Academy of Sciences, Dalian 116023, PR China (Z. Chen).
E-mail addresses: luca.perfetti@polytechnique.edu (L. Perfetti), zwchen@dicp.ac.cn (Z. Chen).

https://doi.org/10.1016/j.apsusc.2025.162564
Received 24 September 2024; Received in revised form 7 January 2025; Accepted 27 January 2025
Available online 28 January 2025

2. Experimental and computational details

Time-resolved ARPES measurements and Potassium (K) atoms deposition from a commercial gettter source were conducted in a high-vacuum chamber with a base pressure of 8×10^{-11} mbar, while maintaining the sample at 130 K. Our experimental setup utilizes a Ti: Sapphire laser system that delivers pulses of 6 μJ with a repetition rate of 250 kHz [16]. This setup includes a laser beam at 1.57 eV with a 50 fs pulse duration, used for pumping the sample, and another laser beam at 6.3 eV generated through cascade frequency mixing in BaB_2O_4 (BBO) crystals, which is employed to probe photoexcited states in the sample. The pump beam injects onto the sample before the probe beam at the positive delay time, while the illumination order of the two beams is opposite at the negative delay time. The sample of InSb (100), mounted on a cryogenic manipulator, was probed using p-polarized light at an incident angle of 45°. Besides, the overall energy resolution of the experiment is ≅ 30 meV, the angle resolution is 0.5° and the cross correlation between pump and probe pulses has full width at half maximum (FWHM) of 160 fs. Before the TrARPES measurements, InSb (100) wafers have been cleaned by means of repeated cycles of Ar ion sputtering and subsequent annealing at 700 K in a high-vacuum chamber, and then were orientated using low energy electron diffraction pattern. In all photoelectron spectra, the energy zero was aligned with the Fermi level, which was referenced to a copper plate in electrical contact with the samples. No charging effects were observed during the measurements.

All DFT calculations were performed using Materials Studio 2017 with the Dmol^3 software [17,18]. The crystal used in this study was cubic with space group $F\bar{4}3$ m, having lattice parameters of a = b = c = 6.63 Å. A generalized gradient approximation was used with the Perdew-Burke-Ernzerhof exchange correlation function [19]. The following configurations were chosen for the geometry optimizations: convergence standards of 10^{-5} Ha on energy, 2×10^{-3} Ha/Å on the force, and 5×10^{-3} Å on displacement. The Brillouin zone was sampled using a 4 × 4 × 4 Monkhorst-Pack grid [20–22]. The electric field is applied exclusively in the direction perpendicular to the (1 0 0) crystal plane and is specified in the format [X 0 0]. (where X is any value in atomic units; 1 atomic unit = 51.42 V/Å). The bands have been shifted to put the maximum of the valence band at 0 eV.

3. Results and discussion

The evaporation of alkali metals onto semiconductor surfaces releases electrons, which accumulate over the band-bending region that extends over at least a few atomic layers, where the field is non-zero. The formation of dipoles is directly proportional to the surface density of alkali atoms [12,13]. Fig. 1 (a) depicts a schematic of an InSb (100) crystal with an external electric field perpendicular to the (100) crystal plane. In general, an external electric field induces the Stark effect and the Stark effect manifests differently at various electric field strengths. As illustrated in Fig. 1(b), both the valence band and conduction band to move in the same direction in energy space under low electric fields, while band gap renormalization occurs under a large electric field. Fig. S1 (a, b) show the Raman spectroscopy and time-resolved ARPES of pristine InSb (100) with a pump fluence of 65 μJ/cm^2 at the positive delay time of 3.5 ps, respectively. The peaks at 191 cm^{-1} and 180 cm^{-1} correspond to LO and TO phonon modes shown in Fig. S1 (a), respectively, which is agreement with the previous study of InSb (100) by Raman spectra [23]. In terms of the probe beam of 6.3 eV, the detected k_z value can be estimated according to the formula of

$$k_2 = (2m(E_k \cos\theta^2 + V_0)/\hbar^2)^{1/2} (1)$$

where m is the electron effective mass along the k_z direction, θ is the emission angle, V_0 is potential parameter, E_k is the kinetic energy of the emitted free electrons and $\hbar$ is reduced Planck constant. The inner potential V_0 is roughly 11 eV [24], the hole effective mass is roughly 0.43 m_o (m_o is free electron mass) [25–27], and the kinetic energy of the emitted electrons from the valence band top is roughly 1.89 eV, therefore the k_z value is roughly 1.21 Å^{-1} when the photon energy of 6.3 eV is normal incidence. The lattice constant of cubic InSb is 6.47 Å (π/6.47 = 0.48 Å^{-1}), which implies that the k_z value is roughly |ΓX|/2.

As shown by the red and blue dotted curves in Fig. S1(b), the fitting curves reproduce the dispersion of both valence and conduction bands along the $\bar{\Gamma}$-$\bar{X}$ direction with a high degree of accuracy. The band dispersion is fitted by a parabolic expression,

$$E = \pm(\delta + (\hbar k_x)^2/2m_x) (2)$$

where E is energy, δ is a constant, m_x is the hole (m_h) or electron (m_e) effective mass, k_x is the wave vector and ħ is the reduced Planck constant. The m_h is roughly 0.431 ± 0.001 m_o, which is agreement with the previous report [25,26], and the m_e is roghly 0.041 ± 0.001 m_o that is larger than the previous data of 0.014 m_o [25,26]. The discrepancy could be attributed to the different k_z values from Γ and the fact that the fit is based on the band edge rather than the band center. The band gap at 130 K is approximately 0.30 eV, determined by the difference between the VBM and CBM acquired at the positive delay time of 3.5 ps. A delay time of 3.5 ps is sufficient to observe the CBM [28]. According to the temperature-dependent bandgap relation studied by Littler et al. [2], the band gap is expected to be approximately 0.22 eV at 130 K. In addition, the exciton binding energy (0.5 meV) of the InSb semiconductor [29], is negligible compared to the band gap of approximately 300 meV. Therefore, the difference of 80 meV is mainly due to our detected k_z value is roughly |ΓX|/2. Next, we started the following K atom doping measurements based on the 0.30 eV band gap.

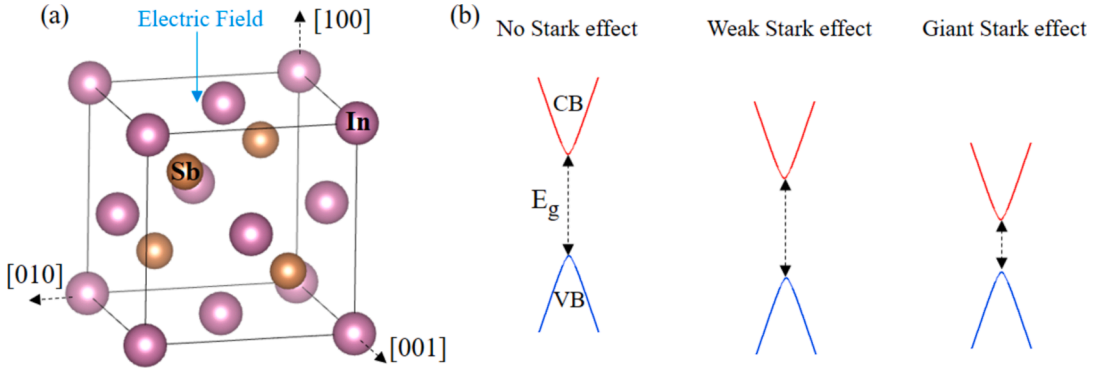

Fig. 1. (a) Schematic of InSb (100) crystal with an external electric field perpendicular to the (100) crystal plane. InSb has a cubic crystal structure. (b) Stark effect under different electric field strengths. CB, VB and E_g represent the conduction band, valence band and band gap between the conduction band bottom and valence band top.

As shown in the second-derivative TrARPES maps (Fig. 2(a-c)) acquired at negative delay time of 0.2 ps at 130 K with a pump fluence of 65 μJ/cm^2 derived from Fig. S2 (a, c, d), the bottom of the conduction band becomes increasingly apparent with longer K atom doping time. At early doping time (Fig. 2(a)), the conduction band could not be visualized by TrARPES at negative delay time, but one can see the downshift of valence band in energy space. Fortunately, the band gap can be obtained by positive second-derivative TrARPES shown in Fig. 2(d) even at early doping time. Fig. 2(d-f) shows corresponding second-derivative K-doping-dependent TrARPES maps acquired at positive delay time of 3.5 ps derived from Fig. S2 (e, g, h). We used second-derivative ARPES maps in the main text of this work. We continued to use the hole effective masses of 0.431 ± 0.001 m_o and electron effective masses of 0.041 ± 0.001 m_o to fit the dispersion of the valence and conduction bands in the second-derivative TrARPES maps. The fitting curves accurately reproduce the dispersion of both bands along the $\overline{\Gamma}$-$\overline{X}$ direction. The band gap is roughly 0.30 eV at the doping time of 1 min. Then, the conduction band bottom can be observed at moderate doping level even without pump light (Fig. 2(b)), and the band gap is 0.25 eV. Finally, the valence band shifts upward and conduction band shift downward relative to the Fermi level, which leads to the band gap renormalization of roughly 0.09 eV ascribed to the giant Stark effect shown in Fig. 2(c). The doping density is proportional to the doping time [13]. Generally, the surface photovoltage (SPV) phenomenon takes place following photoexcitation of a semiconductor. Fig. S3 shows the pump-dependent SPV amplitude in InSb (100) at negative delay time of 0.2 ps. The SPV amplitude is close to saturation at 0.03 eV after irradiation by the pump fluence of 50 μJ/cm^2. In order to clarify the influence of pump pulses on the band movement, all K-doped photoelectron intensity maps shown in Fig. S2(a, b, c, d) were acquired at negative delay time of 0.2 ps.

Fig. 3 (a-d) show the evolution of electronic energy bands of bulk InSb single crystal as a function of the external electric field. For simplicity, we neglected the spin–orbit coupling effect, which resulted in a calculated band gap of approximately 0.6 eV, larger than the actual value of 0.24 eV for pristine InSb (100) at 2 K [2]. In spite of the difference of 0.36 eV, we still observe the band gap renormalization. We set the VBM to 0 eV, and as the electric field increases, the conduction band moves downward in energy and then the band gap decreases. The CBM and VBM nearly overlap when the electric field is 10.8 V/nm, a phenomenon attributed to the Stark effect. Furthermore, the energy level splitting occurs under external electric field in our calculations, which is similar to the early work on the electronic structure modulation of InSb nanowires and nanofilms under external electric field using an eight-band model [30]. The different effects of the Stark field on the heavy-hole valence band, light-hole band, and conduction band could be attributed to their distinct band structures, specifically the varying scattering mechanisms from defects, phonons, and intervalley transitions under external fields [31].

In addition, compared to the band gap, which began to decrease from approximately 0.05 V/nm in the previous study on layered black phosphorus (BP) [13], our value of approximately 2.5 V/nm is significantly larger. Such a significant difference may be attributed to the following factors. First, heavier atoms generally exhibit higher polarizability due to a larger number of electrons and larger atomic size. The

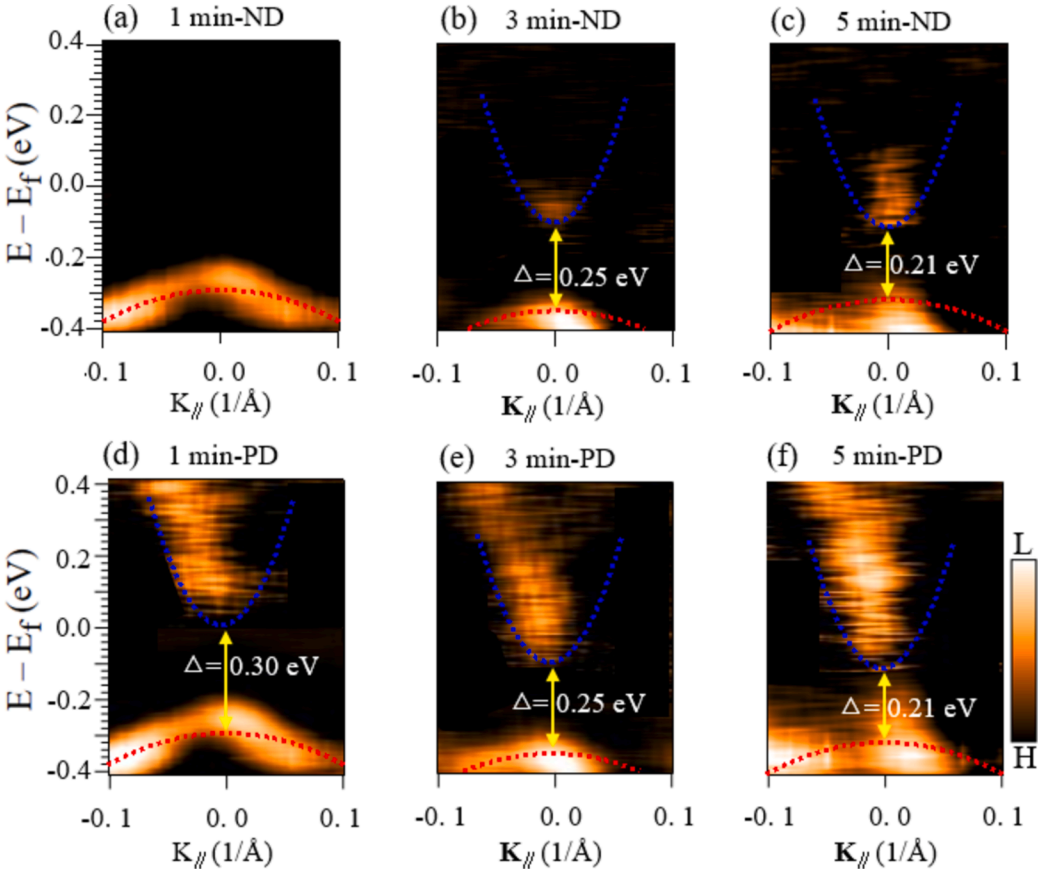

Fig. 2. (a-c) Second-derivative K- doping-dependent TrARPES maps acquired at negative delay time of 0.2 ps at 130 K with a pump fluence of 65μJ/cm^2 derived from Fig. S2 (a, c, d). (d-f) Corresponding second-derivative K- doping-dependent TrARPES maps acquired at positive delay time of 3.5 ps at 130 K with a pump fluence of 65μJ/cm^2 derived from Fig. S2 (e, g, h). We used second-derivative ARPES maps in the main text of this work. ND and PD represent the negative delay time (the pump light of 1.57 eV injects after the probe light of 6.3 eV) and the positive delay time (the pump light of 1.57 eV injects before the probe light of 6.3 eV). We multiplied the signal at a positive energy by a factor of 5 in order to visualize the conduction and valence band on the same color scale. The band gaps are indicated in the panels.

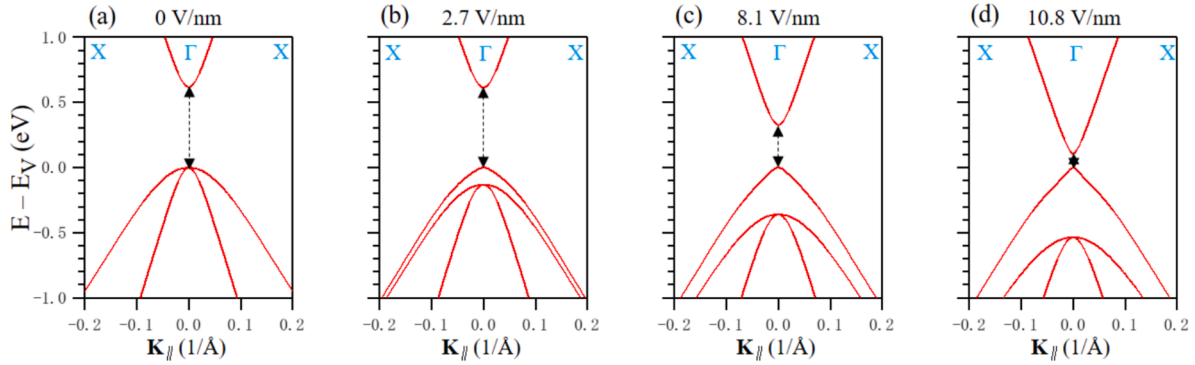

Fig. 3. (a-d) Electronic band structure evolution of bulk InSb along the Γ–X direction as functions of external electric field in the direction perpendicular to the (100) crystal plane. The two-way arrows represent the bandgap between the CBM and VBM.

polarizability of a material can increase with the number of electrons, which is related to the atomic mass. Greater polarizability typically results in a higher dielectric constant. In semiconductors, a higher dielectric constant results in a stronger shielding effect against externally applied electric fields. This is because the dielectric constant indicates the material's ability to polarize in response to an electric field. A rough estimate of the relative polarizability between InSb and BP could be made using the atomic polarizability data (which generally scales with atomic size and number of electrons). Given that In (Atomic number 49) is much heavier than P (Atomic number 15), we expect InSb to have a greater polarizability than BP. Therefore, InSb has a higher dielectric constant than BP. InSb has a dielectric constant of around ϵ_r ~17 at room temperature [32], which is quite high compared to BP, whose dielectric constant varies, but for the anisotropic form, it can be around $\epsilon_r \sim 8 - 12$ along different directions [33]. For a rough estimate, InSb could need the electric field of 2 times stronger than BP to induce a band gap renormalization. Second, the electronic structure of InSb (a III-V semiconductor) and BP (a layered material, like graphene, but with intrinsic anisotropy) is different, which affects how the materials respond to external electric fields. To summarize, the heavier elements in InSb (compared to BP) would indeed affect the Stark effect, likely leading to a stronger screening to the external electric field due to a larger dielectric constant. However, the correction from atomic mass alone is unlikely to explain the full factor of 50 discrepancy. The discrepancy is likely due to additional effects, such as the anisotropic nature of BP, band structure differences, or perhaps an incomplete model for the Stark effect in this context. A more detailed calculation, including specific polarizability data and considering the anisotropy and electronic structure of both materials, would be needed to make a more precise estimate of the correction in future.

4. Conclusions

In conclusion, we investigated the evolution of the band structure of bulk InSb (100) as a function of potassium atom doping density using time-resolved ARPES. Due to the generation of numerous dipoles at the InSb interface, our measurements show both band movement and band gap renormalization, attributed to the Stark effect. In addition, we simulated the external-electric-field-dependent band structure of InSb by DFT calculations. We observed not only a reduction in the band gap but also splitting of the energy levels. Our study provides insights into its optoelectronic properties and potentially enhancing the performance of multifunctional devices using InSb semiconductors.

CRediT authorship contribution statement

Jingwei Dong: Writing – original draft, Methodology, Investigation, Formal analysis, Data curation, Conceptualization. **Yi Lian:** Software, Methodology, Data curation, Conceptualization. **Yongguang Zhang:** Writing – review & editing, Visualization, Validation, Supervision, Resources, Funding acquisition, Formal analysis, Conceptualization. **Luca Perfetti:** Writing – review & editing, Visualization, Validation, Supervision, Software, Resources, Methodology, Investigation, Formal analysis, Conceptualization. **Zhongwei Chen:** Writing – review & editing, Visualization, Validation, Supervision, Software, Resources, Project administration, Methodology, Funding acquisition, Formal analysis, Conceptualization.

Declaration of competing interest

The authors declare that they have no known competing financial interests or personal relationships that could have appeared to influence the work reported in this paper.

Acknowledgements

This work was financially supported by the National Natural Science Foundation of China (Grant No. 22409194), the Energy Revolution S&T Program of Yulin Innovation Institute of Clean Energy (Grant No. YlCE E411060316), the Strategic Priority Research Program of the Chinese Academy of Sciences (Grant No. XDB0600000, XDB0600200) and Natural Science Foundation of Liaoning Province (Grant No.2024BSBA27). The authors express their gratitude Prof. Runze Liu for help in the DFT calculations.

Appendix A. Supplementary material

Supplementary data to this article can be found online at https://doi.org/10.1016/j.apsusc.2025.162564.

Data availability

Data will be made available on request.

References

[1] E. Litwin-staszewska, W. Szymanska, R. Piotrzkowski, The electron-mobility and thermoelectric-power in InSb at atmospheric and hydrostatic pressures, Phys. Status Solidi B Basic Res. 106 (1981) 551–559.
[2] C.L. Littler, D.G. Seiler, Temperature dependence of the energy-gap of InSb using nonlinear optical techniques, Appl. Phys. Lett. 46 (1985) 986–988.
[3] D.L. Rode, Electron transport in InSb, InAs and InP, Phys. Rev. B 3 (1971) 3287–3299.
[4] M. Zimpel, M. Oszwaldowski, J. Goc, Mobility of holes in InSb, Acta Phys. Pol. 75 (1989) 297–300.
[5] C.Y. Zhi, X.D. Bai, E.G. Wang, Synthesis and field-electron-emission behavior of aligned GaAs nanowires, Appl. Phys. Lett. 86 (2005).
[6] H. Kind, H.Q. Yan, B. Messer, M. Law, P.D. Yang, Nanowire ultraviolet photodetectors and optical switches, Adv. Mater. 14 (2002) 158–160.
[7] J.A. del Alamo, Nanometre-scale electronics with III-V compound semiconductors, Nature 479 (2011) 317–323.

[8] S. Ghosh, S.M. Valiyaveettil, G. Shankar, T. Maity, K.-H. Chen, K. Biswas, S. Suwas, R.C. Mallik, Enhanced Thermoelectric Properties of In-Filled Co_4Sb_{12} with InSb Nanoinclusions, ACS Appl. Energy Mater. 3 (2020) 635–646.
[9] O. Gul, H. Zhang, F.K. de Vries, J. van Veen, K. Zuo, V. Mourik, S. Conesa-Boj, M. P. Nowak, D.J. van Woerkom, M. Quintero-Perez, M.C. Cassidy, A. Geresdi, S. Koelling, D. Car, S.R. Plissard, E.P.A.M. Bakkers, L.P. Kouwenhoven, Hard Superconducting Gap in InSb Nanowires, Nano Lett. 17 (2017) 2690–2696.
[10] K. Tomioka, M. Yoshimura, T. Fukui, A III-V nanowire channel on silicon for high-performance vertical transistors, Nature 488 (2012) 189–192.
[11] M. Kang, B. Kim, S.H. Ryu, S.W. Jung, J. Kim, L. Moreschini, C. Jozwiak, E. Rotenberg, A. Bostwick, K.S. Kim, Universal Mechanism of Band-Gap Engineering in Transition-Metal Dichalcogenides, Nano Lett. 17 (2017) 1610–1615.
[12] J. Kim, S.S. Baik, S.H. Ryu, Y. Sohn, S. Park, B.-G. Park, J. Denlinger, Y. Yi, H. J. Choi, K.S. Kim, Observation of tunable band gap and anisotropic Dirac semimetal state in black phosphorus, Science 349 (2015) 723–726.
[13] Z. Chen, J. Dong, C. Giorgetti, E. Papalazarou, M. Marsi, Z. Zhang, B. Tian, Q. Ma, Y. Cheng, J.-P. Rueff, A. Taleb-Ibrahimi, L. Perfetti, Spectroscopy of buried states in black phosphorus with surface doping, 2D Mater., 7 (2020).
[14] Z. Chen, M.-I. Lee, Z. Zhang, H. Diab, D. Garrot, F. Ledee, P. Fertey, E. Papalazarou, M. Marsi, C. Ponseca, E. Deleporte, A. Tejeda, L. Perfetti, Time-resolved photoemission spectroscopy of electronic cooling and localization in $CH_3NH_3PbI_3$ crystals, Phys. Rev. Mater. 1 (2017).
[15] Z. Chen, J. Dong, E. Papalazarou, M. Marsi, C. Giorgetti, Z. Zhang, B. Tian, J.-P. Rueff, A. Taleb-Ibrahimi, L. Perfetti, Band Gap Renormalization, Carrier Multiplication, and Stark Broadening in Photoexcited Black Phosphorus, Nano Lett. 19 (2019) 488–493.
[16] J. Faure, J. Mauchain, E. Papalazarou, W. Yan, J. Pinon, M. Marsi, L. Perfetti, Full characterization and optimization of a femtosecond ultraviolet laser source for time and angle-resolved photoemission on solid surfaces, Rev. Sci. Instrum. 83 (2012).
[17] K. Zhang, Q. Wang, B. Wang, Y. Xu, X. Ma, Z. Li, A DFT study on CO methanation over the activated basal plane from a strained two-dimensional nano-MoS_2, Appl. Surf. Sci. 479 (2019) 360–367.
[18] X. Gui, Q. Zhou, S. Peng, L. Xu, W. Zeng, Adsorption behavior of Rh -doped MoS_2 monolayer towards SO_2, SOF_2, SO_2F_2 based on DFT study, Physica E Low Dimens. Syst. Nanostruct. 122 (2020).
[19] J.P. Perdew, K. Burke, M. Ernzerhof, Generalized gradient approximation made simple Phys, Rev. Lett. 78 (1997) 1396.
[20] H.J. Monkhorst, J.D. Pack, Special points for Brillouin-zone integrations, Phys. Rev. B 13 (1976) 5188–5192.
[21] K.V.K. Rao, S.V.N. Naidu, L. Iyengar, Thermal expansion of rutile and anatase, J. Am. Ceram. Soc. 53 (1970) 124.
[22] N.F. Mott, A.M. Stoneham, Lifetime of electrons, holes and excitons before self-trapping, J. Phys. C: Solid State Phys. 10 (1977) 3391–3398.
[23] C. Seok, M. Choi, S. Park, J. Jung, Y. Park, I.-S. Yang, E. Yoon, Raman Spectroscopy of the Damages Induced by Ar-Ion Beam. Etching of InSb(100) Surface, ECS Solid State Lett. 3 (2014) P27–P29.
[24] S. Yang, N.B.M. Schroeter, V.N. Strocov, S. Schuwalow, M. Rajpalk, K. Ohtani, P. Krogstrup, G.W. Winkler, J. Gukelberger, D. Gresch, G. Aeppli, R.M. Lutchyn, N. Marom, Electronic Structure of InAs and InSb Surfaces: Density Functional Theory and Angle-Resolved Photoemission Spectroscopy, Adv. Quantum Technol 5 (2022).
[25] N. Bouarissa, H. Aourag, Effective masses of electrons and heavy holes in InAs, InSb, GaSb, GaAs and some of their ternary compounds, Infrared Phys Technol. 40 (1999) 343–349.
[26] W. Zawadzki, Electron transport phenomena in small-gap semiconductors, Adv. Phys. 23 (1974) 435–522.
[27] V.N. Strocov, L.L. Lev, F. Alarab, P. Constantinou, X. Wang, T. Schmitt, T.J. Z. Stock, L. Nicolai, J. Ocenasek, J. Minar, High-energy photoemission final states beyond the free-electron approximation, Nat. Commun. 14 (2023).
[28] J. Dong, R. Liu, F. Meng, D. Luo, L. Perfetti, Z. Chen, Femtosecond laser-induced ultrafast electron dynamics and band gap renormalization in InSb, Appl. Surf. Sci. 682 (2025).
[29] W. Liu, A.Y. Chang, R.D. Schaller, D.V. Talapin, Colloidal InSb Nanocrystals, J.am. chem.soc. 134 (2012) 20258–20261.
[30] X.W. Zhang, S.S. Li, J.B. Xia, Semiconductor-metal transition in InSb nanowires and nanofilms under external electric field, Appl. Phys. Lett. 89 (2006).
[31] T.C. Chasapis, Y. Lee, E. Hatzikraniotis, K.M. Paraskevopoulos, H. Chi, C. Uher, M. G. Kanatzidis, Understanding the role and interplay of heavy-hole and light-hole valence bands in the thermoelectric properties of PbSe, Phys. Rev. B 91 (2015).
[32] J.R. Dixon, J.K. Furdyna, Measurement of the static dielectric constant of the InSb lattice via gyrotropic sphere resonances, Solid State Commun 35 (1980) 195–198.
[33] H. Asahina, Y. Maruyama, A. Morita, Optical reflectivity and band structure of black phosphorus, Physica. B + C 117 (1983) 419–421.